DNA Hybridization Detection based on Plasmonic Photonic Crystal Fiber

Mohammad Y. Azab [1], Abed M. Nasr [1], S. S. A. Obayya [1,*] and Mohamed Farhat O. Hameed [1,2,3, *]

[1] Faculty of Engineering, Mansoura University
Mansoura, Egypt, Mansoura, 35516, Egypt

[2] Centre for Photonics and Smart Materials
Zewail City of Science and Technology, October Gardens, 6th of October City, Giza 12578, Egypt
sobayya@zewailcity.edu.eg

[3] Nanotechnology and Nanoelectronics Engineering Program
Zewail City of Science and Technology, October Gardens, 6th of October City, Giza 12578, Egypt
mfarahat@zewailcity.edu.eg

Abstract ─ A novel design of surface plasmon (SP) photonic crystal fiber (PCF) for DNA hybridization detection is proposed and analyzed. The suggested biosensor relies on plasmonic D-shaped PCF configuration. Accordingly, the core guided mode in the silica core is coupled with the SP mode near the plasmonic layer. The resonance wavelength is sensitive to the DNA hybridization process. Therefore, the suggested bio-sensor is studied to maximize the DNA hybridization detection sensitivity by adjusting the structural geometrical parameters. The numerical results are obtained using full vectorial finite element method with perfectly matched layer boundary condition and non-uniform meshing capabilities. The reported D-shaped PCF offers high wavelength sensitivity of 405.4 nm/RIU with a corresponding amplitude sensitivity of 5.65 RIU^{-1}. Consequently, the applications based on DNA classification can be potentially implemented by the reported biosensor.

Index Terms ─ D-shaped fiber, DNA hybridization, photonic crystal fiber, plasmonic biosensor.

I. INTRODUCTION

Photonic crystal fiber (PCF) [1] is one of the most reliable designs in the field of waveguides and optical sensors. PCFs are characterized by their high field confinement, low attenuation loss, high effective mode area and high design flexibility. Further, adding a plasmonic material to the PCF structure allows the coupling between the core guided modes and the surface plasmon (SP) modes. The coupling takes place when the real parts of the effective indices of the core and SP modes are the same. The plasmonic PCFs have been widely used for Glucose level monitoring [2] and cancer early detection [3]. However, it will be used in the current manuscript for DNA hybridization detection which has become of great importance. Through the DNA hybridization process, the single stranded DNA (ssDNA) is transformed into double stranded DNA (dsDNA) when the two complement ssDNA sequences are merged together. To detect the hybridization process, two techniques can be used, namely label free and label-based. The label based mechanism requires a complex handling for the liquid along with labeling procedure with a long assay time. Therefore, the label-free procedure is highly needed for monitoring bimolecular interaction in real time without the labeling process. A slot-waveguide biosensor based on label-free mechanism for detecting DNA hybridization has been suggested with sensitivity of 856 nm/RIU and a corresponding detection-limit of 1.43×10^{-6} RIU [4]. In addition, Yin *et al.* [5] have investigated a thin-core fiber based modal interferometer DNA sensor. Such a sensor is based on layer-by-layer self-assembly where a sensitivity of 0.27 nm/matched-base has been obtained at a concentration of 1 mM. Further, an interferometric reflectance imaging sensor has been suggested to quantify the mass density for DNA [6]. Furthermore, a sensitivity of 893.5 nm/RIU has been achieved using a horizontal slot waveguide biosensor with a ring resonator arrangement [7]. However, the analysis of the proposed designs in [4, 7] does not study the whole system with the suggested micro-ring resonator. Moreover, a microfiber Bragg grating (mFBG) was presented as a sensing probe for DNA hybridization detection with a surrounding refractive index (SRI) resolution up to 2.6×10^{-5} RIU [8]. Additionally, an in-line fiber Michelson interferometer based optofluidic biosensor was proposed for the detection of DNA hybridization with a detection limit of 5 nano-Mole (nM)

Submitted On: May 10, 2020
Accepted On: February 6, 2021
https://doi.org/10.47037/2020.ACES.J.360301

[9]. Further, a microfiber Bragg grating (mFBG) based reflective fiber-optic biosensor has been investigated in [10] for DNA hybridization detection using layer-by-layer self-assembly technology. Recently, PCF biosensor has been proposed with plasmonic rod for the detection of DNA hybridization with a sensitivity of 94.59 nm/RIU [11]. In addition, Kaye *et al.* [12] have used a localized SPR (LSPR) coupled fiber-optic (FO) nano-probe for the detection of DNA hybridization and DNA concentrations with detection limit of 10 fM. Moreover, a highly sensitive hybrid plasmonic slot-waveguide (HPSW) biosensor based on silicon-on-insulator was proposed by Hameed *et al*. [13] for DNA hybridization detection. Such a sensor [13] is characterized by sensitivity of 1890.4 nm/RIU and a detection-limit of 2.65×10^{-6} RIU. However, the HSPW has a complex structure for fabrication.

In this paper, a D-shaped PCF biosensor is presented and analyzed for detecting DNA hybridization process. The proposed design achieves wavelength and amplitude sensitivities of 405.4 nm/RIU and 5.65 RIU^{-1}, respectively. Further, the suggested D-shape design has the advantage of fabrication simplicity with higher sensitivity than 94.59 nm/RIU of that presented in [11]. Further, the reported sensor relies on the widely fabricated hexagonal PCF with a great capability for applications based on DNA classification.

II. NUMERICAL TECHNIQUE

In this study, full vectorial finite element method (FVFEM) [14, 15] is used for the modal analysis of the suggested DNA biosensor. Based on Maxwell's equations, the following magnetic field based vector wave equation can be expressed as:

$$\nabla \times (\varepsilon^{-1} \nabla \times \mathrm{H}) - \omega^2 \mu_0 \mathrm{H} = 0, \qquad (1)$$

where μ_0 is the free space permeability and ω is the angular frequency. In addition, $\varepsilon = \varepsilon_0 \varepsilon_r$ is the waveguide material permittivity where ε_r is the relative permittivity and ε_0 is the free space permittivity. By applying the standard finite element method to the wave equation, the following eigenvalue equation can be obtained:

$$[\mathrm{K}]\{\mathrm{H}\} - \beta^2[\mathrm{M}]\{\mathrm{H}\} = \{0\}, \qquad (2)$$

where [H] is the global magnetic field vector, [M] and [K] are the global mass and stiffness matrices, β is the propagation constant and $\{0\}$ is the null vector. By solving the eigenvalue equation, the eigenvalue β and the wave vector H can be determined. Moreover, the propagation constant β for a specific mode is used to calculate the effective index via $n_{eff} = \beta/k$, given that k is the wavenumber of free space. In this study, the FVFEM is used via Comsol Multiphysics 5.4 software package [16]. Through the modal analysis of the suggested biosensor, non-uniform meshing is used with minimum element size of $1.12 \times 10^{-4}\ \mu m$. Further, 399217 degrees of freedom are employed to maximize the calculation accuracy and save the computation cost. An AMD dual-core computer processor at 2.9 GHz with 8.0 GB RAM and 64-bit operating system has been used to run the software with an average runtime of 120 seconds/run.

III. DESIGN CONSIDERATIONS AND NUMERICAL RESULTS

To justify our choice of the D-shape configuration, a complete ring–shaped PCF biosensor design will be first considered as shown in Fig. 1 (a). The sensor is based on one ring of hexagonal lattice PCF with a solid core and silica background material. The proposed PCF biosensor has air holes diameter d and a hole pitch Λ while the silver layer has a thickness t. An additional air hole of diameter $d_s = 0.3d$ is also added at a distance $d_y = 0.65\,\Lambda$ below the center to enhance the biosensor sensitivity. It may be seen from Fig. 1 (a) that the silver layer is deposited on the outer surface of the PCF followed by a linker layer which attracts the DNA strands. The linker layer consists of silane with 1 nm thickness and 1.42 index of refraction. Further, the DNA strands are added after the linker layer. According to [4], the thickness of the DNA layer before (ssDNA) and after (dsDNA) the hybridization process is the same value of 8 nm. Moreover, the refractive indices of the ssDNA and dsDNA layers are equal to 1.456 and 1.53, respectively. Further a water layer of refractive index 1.33 is added where the DNA strands are inserted. Additionally, the computational domain is truncated by using PML layer.

The relative permittivity of silica glass ε_s is dependent on the wavelength λ in μm via [11]:

$$\varepsilon_s = 1 + \frac{B_1\lambda^2}{\lambda^2 - C_1} + \frac{B_2\lambda^2}{\lambda^2 - C_2} + \frac{B_3\lambda^2}{\lambda^2 - C_3}, \qquad (3)$$

where the constants B_3, B_2 and B_1 have values of 0.8974794, 0.4079426 and 0.6961663, respectively. On the other hand, C_3, C_2 and C_1 are equal to 97.9340025 μm^2, 0.0135120631 μm^2 and 0.00467914826 μm^2, respectively. Additionally, the relative permittivity of the silver can be obtained using the following Drude-Lorentz model [17]:

$$\varepsilon_{Ag} = 1 - \frac{\Omega_p^2}{\omega(\omega - i\Gamma_0)} + \sum_{j=1}^{k} \frac{f_j \omega_p^2}{\left(\omega_j^2 - \omega^2\right) + i\omega\Gamma_j}, \qquad (4)$$

where ω_p is the plasma frequency, k is the number of oscillators with frequency ω_j, strength f_j, and lifetime $1/\Gamma_j$, while $\Omega_p = \sqrt{f_0}\omega_p$ is the plasma frequency associated with intraband transitions with oscillator strength f_0 and damping constant Γ_0.

Figure 1 (b) shows the wavelength dependence of the real parts of the effective index of the transverse magnetic (TM) SP mode and the TM core guided mode. Additionally, the confinement loss for the quasi TM core guided mode is also presented in Fig. 1 (b). The study is carried out at $\Lambda = 1.2$ μm, $d = 0.56$ μm, $t = 70$ nm and

ssDNA layer with index of refraction of 1.456. The inset of Fig. 1 (b) shows that at $\lambda = 700$ nm away from the coupling wavelength, the quasi TM core guided mode has a good confinement to the core region. Accordingly, the real parts of the effective index of both the core guided and the SP modes are away from each other and no coupling occurs. On the other hand, at $\lambda = 745$ nm, the real parts of the effective index of both the quasi TM core guided mode and SP mode are the same. As a result, the power transfer to the SP mode from the core mode is maximum where the quasi TM core guided mode is less confined in the core region as shown in the inset of Fig. 1 (b).

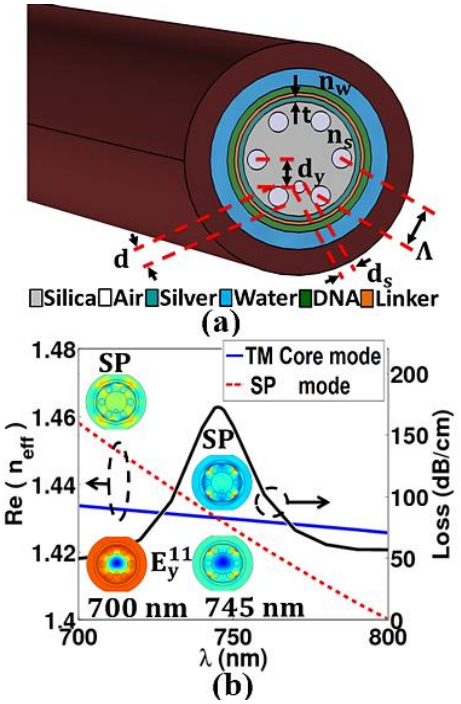

Fig. 1. (a) 3D schematic diagram of ring shaped DNA SPR PCF biosensor, and (b) Effective indices of the main component of the SP mode and the quasi TM core mode along with the confinement losses of the TM core mode as a function of the wavelength at $n_{DNA} = 1.456$. The inset shows field plots of the SP mode and the fundamental components of the quasi TM core mode at wavelengths of 700 nm and 745 nm.

The sensitivity of the suggested DNA sensor to the degree of hybridization is tested via the interrogation methods for both the wavelength and amplitude. The wavelength sensitivity can be calculated via the change in the resonance wavelength for the two DNA cases (n=1.456 for ssDNA and n=1.53 for dsDNA) [4] as follows [2]:

$$S_\lambda = \partial\lambda_0(n_{DNA})/\partial n_{DNA}\,, \quad \text{nm/RIU} \qquad (5)$$

where λ_0 is the resonance wavelength for a specific DNA refractive index n_{DNA}. Additionally, the amplitude sensitivity (RIU^{-1}) can be obtained using the following equation [2]:

$$S_A = -\frac{\partial\alpha(\lambda, n_{DNA})/(\partial n_{DNA})}{\alpha(\lambda, n_{DNA})}\,, \qquad (6)$$

where $\alpha(\lambda, n_{DNA})$ is the confinement loss of the core guided mode as a function of the DNA refractive index n_{DNA} and wavelength λ. Unfortunately, the numerical study results in very low wavelength and amplitude sensitivities of 13.5 nm/RIU and 0.33 RIU^{-1}, respectively. Accordingly, to enhance the sensitivity of the DNA biosensor, a horizontal etching is applied on the PCF to obtain a D-shaped SPR PCF as shown in Fig. 2 (a). The D-shape is obtained by removing two rows of the air holes via horizontal etching. The core region is obtained by introducing a solid silica rod instead of a capillary in the central region. The proposed PCF structure has a hexagonal lattice with air holes diameter d and a hole pitch Λ as presented in Fig. 2 (a). Further, a silver layer of thickness t is deposited on the etched surface which serves as a plasmonic material. Additionally, a layer of silane with thickness 1 nm and refractive index of 1.42 is added above the silver as a linker layer for DNA strands.

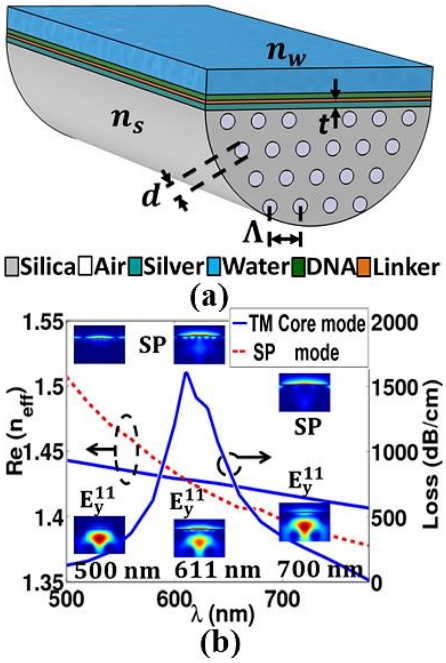

Fig. 2. (a) 3D schematic diagram of D-shaped DNA SPR PCF biosensor, and (b) effective indices of the main component of the SP mode and the quasi TM core mode along with the confinement losses of the TM core mode as a function of the wavelength at $n_{DNA} = 1.456$. The inset shows field plots of the SP mode and the fundamental components of the quasi TM core mode at wavelengths of 500 nm, 611 nm and 700 nm.

It is worth noting that the thickness of the DNA layer before and after the hybridization process has the same value of 7 nm [4]. Additionally, the DNA layer is surrounded by a water of refractive index 1.33. The modal analysis is performed on a computational domain of rectangular shape having a width 11.04 μm and a height 9.05 μm with a PML boundary condition. Further, minimum element size of 0.000232 μm and 305113 degrees of freedom are used to describe the used non uniform mesh. Due to the horizontal etching of the plasmonic D-shaped PCF, only TM modes are considered in the following study. The dependency of the real parts of the effective indices of the SP mode and the TM core guided mode along with the confinement loss for the quasi wavelength dependent TM core guided mode are presented in Fig. 2 (b). This investigation is performed at $\Lambda = 1.2\ \mu m$, $d = 0.6\ \mu m$, $t = 70\ nm$ with a ssDNA layer of refractive index 1.456. The field plots in the inset of Fig. 2 (b) clarify that away from the coupling wavelength (500 nm and 700 nm), the TM core guided mode is well confined to the core region where no coupling is obtained between the core guided mode and the SP mode. However, at the coupling wavelength of 611 nm, both the SP mode and the TM core guided mode have the same effective index. Accordingly, the confinement loss has its maximum value at the coupling wavelength of 611 nm. The suggested D-shaped DNA biosensor's sensitivity is optimized by controlling the structural geometrical parameters such as the hole pitch Λ, the air holes diameter d and the silver layer thickness t. First, the hole pitch is considered with the following values: 1.2 µm, 1.3 µm and 1.4 µm while the air hole diameter and the silver thickness are kept constant at 0.6 µm and 70 nm, respectively. Figure 3 represents the wavelength dependence of the loss spectra along with the amplitude sensitivity for ssDNA and dsDNA at different hole pitch values. It can be realized from Fig. 3 (a) that at $\Lambda = 1.2$ µm, the coupling wavelength is found at 611 nm for the ssDNA ($n_{DNA} = 1.456$), while the dsDNA case ($n_{DNA} = 1.53$) has a resonance wavelength of 630 nm. The resultant shift in the wavelength is equal to 19 nm and the corresponding wavelength sensitivity is 256.75 nm/RIU. In addition, the amplitude sensitivity for the same Λ is equal to 5.66 RIU^{-1} as shown in Fig. 3 (d). At $\Lambda = 1.3$ µm, the resonance wavelength has a blue shift to 602 nm and 617 nm for the ssDNA and dsDNA, respectively. Accordingly, Figs. 3 (b) and (e) show that both the amplitude and wavelength sensitivities are decreased to 5.06 RIU^{-1} and 202.70 nm/RIU, respectively. When $\Lambda = 1.4$ µm is used, the resonance wavelengths have further blue shifts as may be seen from Fig. 3 (c) to 593 nm and 610 nm for ssDNA and dsDNA, respectively. Figures 3 (c) and (f) reveal that the corresponding amplitude and wavelength sensitivities are equal to 5.79 RIU^{-1} and 229.72 nm/RIU, respectively. Therefore, the hole pitch will be kept constant at 1.2 µm with high sensitivity of 256.75 nm/RIU in the subsequent simulations. The same study is carried out for silver layer thickness with three values of 60 nm, 70 nm and 80 nm while the air holes diameter and hole pitch are fixed at 0.6 μm and 1.2 μm, respectively. Figure 4 shows the amplitude sensitivity and confinement loss as a function of the wavelength for different silver layer thicknesses. Figure 4 (a) and shows that at $t = 60$ nm, the resonance occurs at λ=611 nm and 627 nm, respectively. Consequently, the obtained S_A and S_λ are equal to 7.71 RIU^{-1} and 216.21 nm/RIU, respectively. At a silver layer thickness of 70 nm, the resonance wavelength has the same value for ssDNA (611 nm) and a slight increase for dsDNA (630 nm).

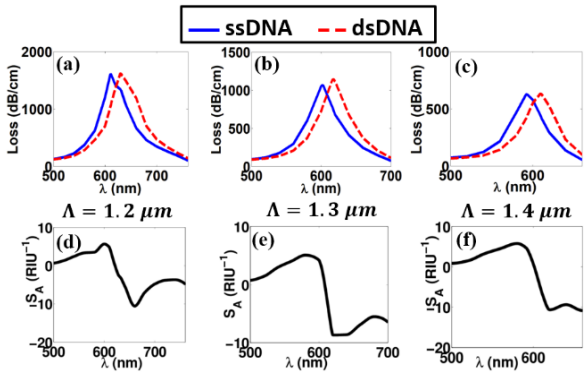

Fig. 3. Confinement losses for the quasi TM core mode and amplitude sensitivity as a function of the wavelength for ssDNA and dsDNA layers at different values of Λ.

Therefore, an increase in the wavelength sensitivity to 256.75 nm/RIU is realized while the obtained S_A is reduced to 5.66 RIU^{-1} as may be seen from Figs. 4 (b) and (e). Further, Fig. 4 (c) reveals that the resonance wavelengths are similar to that of 60 nm at a silver thickness of 80 nm. As a result, the obtained wavelength sensitivity has the same value of 216.21 nm/RIU while a further decrease in the amplitude sensitivity to 3.6 RIU^{-1} is obtained as shown in Fig. 4 (f). The next study is concerned with the diameter of the air holes with values of 0.52 μm, 0.56 μm and 0.60 μm, where the hole pitch and silver layer thickness are kept constant at 1.2 μm and 70 nm, respectively. It may be seen from Fig. 5 (a) that at $d = 0.52\ \mu m$, the coupling occurs at wavelengths of 609 nm and 636 nm for ssDNA ($n_d = 1.456$) and dsDNA ($n_d = 1.53$), respectively. Therefore, the corresponding amplitude and wavelength sensitivities are equal to 7.69 RIU^{-1} and 364.68 nm/RIU, respectively as observed from Figs. 5 (a), (d). It may be also observed from Fig. 5 (b) that using air holes diameter of 0.56 μm could shift the resonance wavelengths to 610 nm and 640 nm for ssDNA ($n_d = 1.456$) and dsDNA ($n_d = 1.53$), respectively. Accordingly, a high wavelength sensitivity of 405.4 nm/RIU is obtained while a slight decrease in

the amplitude sensitivity to 5.62 RIU^{-1} is realized from Figs. 5 (b) and (e). When the air holes diameter is increased to 0.6 μm, the resonance is obtained at 611 nm for ssDNA and 630 nm for dsDNA. The corresponding wavelength sensitivity is decreased to 256.75 nm/RIU while the amplitude sensitivity is nearly the same.

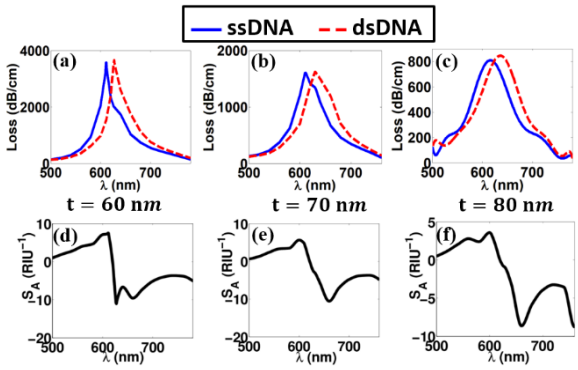

Fig. 4. Confinement losses for the quasi TM core mode and amplitude sensitivity as a function of the wavelength for ssDNA and dsDNA layers at different values of silver layer thickness t.

The suggested D-shaped PCF DNA biosensor is based on silica glass hexagonal lattice which can be fabricated using the well-known stake and draw method [18] where the air holes can be arranged with high accuracy. Additionally, the D-shaped configuration can be accomplished via fiber polish where splicing is applied for long PCF between two single-mode fibers. Then, the spliced fiber is fixed by using a pair of fiber holders. Additionally, the polishing length and depth is accurately controlled by a computer program. Moreover, the silver nano-layer can be obtained using thermal evaporation, sputtering technique and wet-chemistry technique [3]. Further, surface roughness can be minimized via employing chemical vapor deposition (CVD) technique [1]. It is worth noting that slot waveguides biosensors [4, 7, 13] have complex structures with very small geometrical parameters and different layers of different materials. In addition, the coupling to the slot waveguide with a photonic strip-slot waveguide is needed which suffers from undesired back-reflection. Further, mode conversion may occur at the coupling interface which decreases the biosensor sensitivity [19]. In addition, the design in Ref. [11] is based on gold nanowires infiltration which is considered also of high complexity. Further, the technique used in calculating the sensitivity in the slot waveguide designs is based on obtaining the shift in the resonance wavelength via the difference in the effective index of the fundamental core mode. On the other hand, the design of Ref. [11] and the current design are based on obtaining the actual shift in the resonance peek of the confinement loss. Accordingly, the current design uses a more applicable and accurate technique. Moreover, the actual shift in the resonance wavelength for the current design (30 nm) is far higher than any of the preceding designs. Therefore, the sensitivity value of the current design has more reality than those of the other designs.

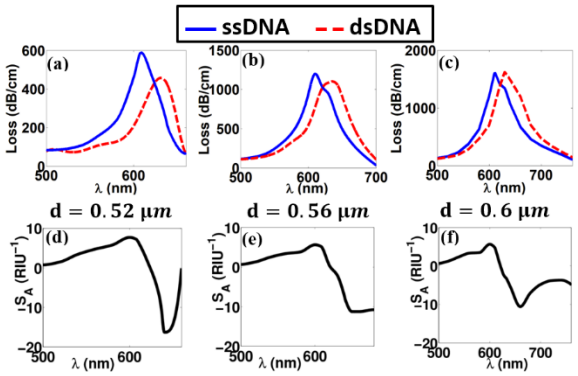

Fig. 5. Confinement losses for the quasi TM core mode and amplitude sensitivity as a function of the wavelength for ssDNA and dsDNA layers at different values of d.

IV. CONCLUSION

An innovative structure of SPR PCF biosensor for DNA hybridization detection is proposed and analyzed. The reported design is based on D-shaped configuration with high amplitude and wavelength sensitivities of 5.65 RIU^{-1} and 405.4 nm/RIU, respectively. Further, the suggested DNA biosensor has advantage in terms of simplicity for the fabrication process. Therefore, the applications based on DNA classification can be potentially implemented by the proposed biosensor with simple and efficient label free technique.

REFERENCES

[1] P. J. Sazio, A. Amezcua-Correa, C. E. Finlayson, J. R. Hayes, T. J. Scheidemantel, N. F. Baril, B. R. Jackson, D. J. Won, Zhang, F. Margine, E. R. V. Gopalan, V. H. Crespi, and J. V. Badding, "Micro-structured optical fibers as high-pressure micro-fluidic reactors," *Science*, vol. 311, no. 5767, pp. 1583-1586, Mar. 2006.

[2] M. Y. Azab, M. F. O. Hameed, and S. S. A. Obayya, "Multi-functional optical sensor based on plasmonic photonic liquid crystal fibers," *Opt. Quant. Electron.*, vol. 49, no. 2, pp. 1-17, Jan. 2017.

[3] A. A. Rifat, R. Ahmed, A. K. Yetisen, H. Butt, A. Sabouri, G. A. Mahdiraji, S. H. Yun, and F. R. M. Adikan, "Photonic crystal fiber based plasmonic sensors," *Sensor. Actuator. B Chem.*, vol. 243, pp. 311-325, May 2017.

[4] T. Dar, J. Homola, B. M. A. Rahman, and M. Rajarajan, "Label-free slot-waveguide biosensor for the detection of DNA hybridization," *Applied*

Optics, vol. 51, no. 34, pp. 8195-8202, Nov. 2012.

[5] M. J. Yin, C. Wu, L. Y. Shao, W. K. E. Chan, A. P. Zhang, C. Lu, and H. Y. Tam, "Label-free, disposable fiber-optic biosensors for DNA hybridization detection," *Analyst*, vol. 138, no. 4, pp. 1988-1994, Jan. 2013.

[6] S. Ahn, D. S. Freedman, X. Zhang, and M. S. Unlü, "High-throughput label-free detection of DNA hybridization and mismatch discrimination using interferometric reflectance imaging sensor," *Methods in Molecular Biology*, vol. 1039, pp. 181-200, July 2013.

[7] C. Viphavakit, M. Komodromos, C. Themistos, W. S. Mohammed, K. Kalli, and B. M. A. Rahman, "Optimization of a horizontal slot waveguide biosensor to detect DNA hybridization," *Applied Optics*, vol. 54, no. 15, pp. 4881-4888, May 2015.

[8] Y. Cao, T. Guo, X. Wang, D. Sun, Y. Ran, X. Feng, and B. O. Guan, "Resolution-improved in situ DNA hybridization detection based on microwave photonic interrogation," *Opt. Express*, vol. 23, no. 21, pp. 27061-27070, Oct. 2015.

[9] R. Gao, D. F. Lu, J. Cheng, Y. Jiang, L. Jiang, J. D. Xu, and Z. M. Qi, "Fiber optofluidic biosensor for the label-free detection of DNA hybridization and methylation based on an in-line tunable mode coupler," *Biosensors and Bioelectronics*, vol. 15, no. 86, pp. 321-329, Dec. 2016.

[10] D. Sun, T. Guo, and B. O. Guan, "Label-free detection of DNA hybridization using a reflective microfiber Bragg grating biosensor with self-assembly technique," *Journal of Lightwave Technology*, vol. 35, no. 16, pp. 3354-3359, Aug. 2017.

[11] M. Y. Azab, M. F. O. Hameed, A. M. Nasr, and S. S. A. Obayya, "Label free detection for DNA hybridization using surface plasmon photonic crystal fiber biosensor," *Optical and Quantum Electronics*, vol. 50, no. 68, pp. 1-13, Jan. 2018.

[12] S. Kaye, Z. Zeng, M. Sanders, K. Chittur, P. M. Koelle, R. Lindquist, U. Manne, Y. Lin, and J. Wei, "Label-free detection of DNA hybridization with a compact LSPR-based fiber-optic sensor," *Analyst*, vol. 142, pp. 1974-1981, Apr. 2017.

[13] M. F. O. Hameed, A. S. Saadeldin, E. M. A. Elkaramany, and S. S. A. Obayya, "Label-free highly sensitive hybrid plasmonic biosensor for the detection of DNA hybridization," *Journal of Lightwave Technology*, vol. 35, no. 22, pp. 4851-4858, Nov. 2017.

[14] S. S. A. Obayya, B. M. A. Rahman, and H. A. El-Mikati, "New full-vectorial numerically efficient propagation algorithm based on the finite element method," *Journal of Lightwave Technology*, vol. 18, no. 3, pp. 409-415, Mar. 2000.

[15] S. S. A. Obayya, B. M. A. Rahman, K. T. V. Grattan, and H. A. El-Mikati, "Full vectorial finite-element-based imaginary distance beam propagation solution of complex modes in optical waveguides," *Journal of Lightwave Technology*, vol. 20, no. 6, pp. 1054-1060, June 2002.

[16] COMSOL Multiphysics® [Online] Available: http://www.comsol.com. COMSOL AB, Stockholm, Sweden"

[17] A. D. Rakic, A. B. Djurisic, J. M. Elazar, and M. L. Majewski, "Optical properties of metallic films for vertical-cavity optoelectronic devices," *Applied Optics*, vol. 37, no. 22, pp. 5271-5283, Aug. 1998.

[18] P. Russell, "Photonic crystal fibers," *Science*, vol. 299, no. 5605, pp. 358-362, Jan. 2003.

[19] V. M. N. Passaro and M. La-Notte, "Optimizing SOI slot waveguide fabrication tolerances and strip-slot coupling for very efficient optical sensing," *Sensors*, vol. 12, no. 3, pp. 2436-2455, Feb. 2012.